Effect of Nanoalumina (Al_2O_3) Filler on the Properties of Poly(Methyl Methacrylate) (PMMA)/50% Epoxidized Natural Rubber (ENR 50) Electrolytes

Nur 'Ain Habep[1], Nabilah Akemal Muhd Zailani[1*], Intan Qhuzairin Zaharuddin[1], Khuzaimah Nazir[1], Fadiatul Hasinah Muhammad[2], Solhan Yahya[1], Fazni Susila Abdul Ghani[3] and Famiza Abdul Latif[3]

[1]Faculty of Applied Sciences, Universiti Teknologi MARA, Cawangan Perlis, Kampus Arau, 02600 Arau Perlis, Malaysia

[2]Centre of Foundation Studies, Selangor, Kampus Dengkil, 43800 Dengkil, Selangor, Malaysia

[3]Faculty of Applied Sciences, Universiti Teknologi MARA, 40450 Shah Alam, Malaysia

*****Corresponding author (e-mail: nabilahakemal@uitm.edu.my)

The effects of various weight percentages (%) (i.e.: 1, 3, 5, 7 and 10 wt. %) of nanoalumina (Al_2O_3) filler (<50 nm) on the structural, electrical, morphological and thermal properties of PMMA/ENR50-based electrolyte films were investigated. The polymer electrolyte films were prepared using the solution casting technique and a fixed amount of LiTf (40 wt.%) was added as the conducting species. With the addition of up to 3 wt. % of Al_2O_3, flexible and free-standing PMMA/ENR50-based electrolyte films ($PMMAF_1$ and $PMMAF_3$) were obtained. The phase separation that naturally occurred in PMMA/ENR50 films also disappeared when observed under an optical microscope (OM). FTIR studies confirmed the occurrence of polymer-salt-filler interactions which successfully increased the amorphicity of the system. This eased the mobility of the Li^+ ions, resulting in the highest ionic conductivity value of 4.36×10^{-4} S/cm for $PMMAF_3$. The filler-salt interactions also improved conductivity by creating new Li^+ conducting pathways. $PMMAF_1$ and $PMMAF_3$ also exhibited higher decomposition temperatures compared to $PMMAF_0$, which could be related to the PMMA-filler interactions as confirmed by FTIR analysis.

Keywords: PMMA; ENR 50; filler; nanoalumina; Al_2O_3; lithium triflate

Received: June 2023; Accepted: August 2023

Lithium-ion batteries commonly contain liquid electrolytes as they have high ionic conductivity and stable interactions with different types of electrodes. However, liquid electrolytes face safety issues due to leakage as well as flammability, and also have a narrow electrochemical stability window [1-2]. These drawbacks limit their performance in lithium-ion batteries. In this study, we focused on polymer electrolytes (PE) as they are safe, non-flammable and do not leak [3], while having other features such as great mechanical strength, lightness, excellent ionic conductivity and high electrochemical stability [4].

Poly(methyl methacrylate) (PMMA) is the most widely used polymer host for PE due to its stability towards the electrode [2,5]. Unfortunately, the substituents on the α-carbon atom of PMMA restrict the chain flexibility of its film, which results in poor electrode-electrolyte contact, thereby reducing ionic conductivity [6]. The polymer blend method is the easiest method to improve the brittleness of PMMA-electrolyte film [4,7]. Latif *et al.* [5] reported that blending PMMA with 50 % epoxidized natural rubber (ENR 50) lowered the glass transition temperature (T_g) of PMMA, produced rubber-like properties, great elasticity and excellent adhesion properties which then increased ionic conductivity. However, the PMMA/ENR 50 polymer blend was not homogenous due to the presence of carbonyl groups in PMMA and polar epoxy groups in ENR 50 that were vulnerable to physical interchain crosslinking by hydrogen bonding [8].

To improve homogeneity and phase separation in the polymer blend, an inorganic filler was added to the system. As previously reported, the incorporation of nanoscale ceramic fillers (i.e., SiO_2, Al_2O_3, and TiO_2) may improve the ionic conductivity, mechanical strength and stability of the polymer electrolyte [9]. However, agglomeration tends to occur when more filler is added, which prevents ion transportation in the polymer electrolyte system. Thus, in this work, different weight percentages (i.e.: 1, 3, 5, 7 and 10 wt. %) of Al_2O_3 nanofiller were added to a PMMA/ ENR 50 blend system. The solution casting technique was used due to its simplicity [8]. The effects of different amounts of Al_2O_3 on the structural, electrical, morphological and thermal properties of the PMMA/ENR 50-based electrolyte system were investigated via Fourier Transform Infrared Spectroscopy (FTIR), Electrochemical Impedance Spectroscopy (EIS), Optical Microscopy (OM) and Thermogravimetric Analysis (TGA), respectively.

EXPERIMENTAL

Chemicals and Materials

Poly(methyl methacrylate) (PMMA) (Molecular weight (M_w): 120,000 g/mol), nanoalumina (Al_2O_3) filler (<50 nm), lithium triflate (LiTf) (Purity: 99.995 %) and analysis grade tetrahydrofuran (THF) were purchased from Merck (Darmstadt, Germany) while 50 % epoxidized natural rubber (ENR 50) was obtained from Lembaga Getah Malaysia (LGM). All these chemicals were used without further purification.

Preparation of PMMA/ENR 50-based Electrolyte Films

The preparation of PMMA/ENR 50-based electrolyte films by the solution casting technique was adapted from Zamri *et al.* [8]. PMMA, ENR 50, LiTf and Al_2O_3 were dissolved separately in THF using magnetic stirrers. There was no heat applied, except in the case of Al_2O_3 which was dissolved at 50 °C. The amount of ENR 50 and the LiTf salt in PMMA were fixed at 10 % and 40 %, respectively, as these compositions were reported to be the most conducting [10]. Various amounts of Al_2O_3 were then added to the mixtures which were stirred continuously at 50 °C until dissolution, which was confirmed by the formation of a homogenous solution with no phase separation. Then, the solutions were cast into petri dishes and left to dry for 24 hours in a fume hood. The films formed were peeled off and kept in an oven at 50 °C for one hour. The films obtained were then stored in a desiccator prior to further characterization. Blank PMMA, blank ENR 50 and PMMA/ENR 50 films were also prepared as controls. The systems with 0, 1, 3, 5, 7 and 10 wt. % of Al_2O_3 were labelled $PMMAF_0$, $PMMAF_1$, $PMMAF_3$, $PMMAF_5$, $PMMAF_7$, and $PMMAF_{10}$, respectively.

Characterization Methods

Fourier Transform Infrared Spectroscopy (FTIR)

The interactions between the constituents of the polymer electrolyte films were investigated using a Perkin Elmer Attenuated Total Reflectance (ATR)-FTIR instrument. The measurements were carried out at a frequency range of 4000 – 600 cm^{-1} with a resolution of 2 cm^{-1} and 16 scans.

Electrochemical Impedance Spectroscopy (EIS)

The ionic conductivity of the polymer electrolyte film was determined using EIS (HIOKI 35232-01 LCR). Prior to measurement, a micrometre screw gauge was used to measure the thickness of the electrolyte film. Then, the film was placed between the two stainless steel blocking electrodes. Impedance at room temperature was measured in the frequency range between 100 Hz – 1 MHz. The bulk resistance (R_b) of the sample was determined from the impedance plots obtained and the ionic conductivity (σ) values of the samples were calculated using equation (1),

$$\sigma = \frac{l}{R_b \cdot A} \quad (1)$$

where R_b is the bulk resistance (Ω), l is the thickness of the film (cm) and A is the effective contact area of the electrode and the electrolyte (cm^2).

From the impedance data, the dielectric constant (ε_r) and dielectric loss (ε_r) values were obtained from equations (2) and (3), respectively.

$$\varepsilon_r = \frac{Z_i}{\omega \cdot C_0 (Z_r^{\ 2} + Z_i^{\ 2})} \quad (2)$$

$$\varepsilon_i = \frac{Z_r}{\omega \cdot C_0 (Z_r^{\ 2} + Z_i^{\ 2})} \quad (3)$$

where C_0 is equal to $\varepsilon_0 A/t$, ε_0 is the permittivity of free space (8.85×10^{-4} cm^{-1}) and ω is the angular frequency ($\omega = 2\pi f$).

Optical Microscope (OM)

An optical microscope (Nikon ECLIPSE ME 600) was used to observe the morphology of the films at 10× magnification.

Thermogravimetric Analyzer (TGA)

Thermogravimetric analysis was carried out using a Pyris 1 Perkin Elmer Thermogravimetric Analyser. 3 mg of film was placed in an aluminium pan and heated from room temperature to 500 °C at a rate of 10 °C min^{-1} under a nitrogen atmosphere.

RESULTS AND DISCUSSION

Formation of PMMA/ENR 50-based Electrolyte Films

The PMMA film obtained in Figure 1(a) was brittle. This may be caused by the restricted flexibility of the PMMA chain due to substituents at the α-carbon atom [6]. Figure 1(b) shows the ENR 50 film which was sticky and could not be peeled off the Petri dish. This was due to the epoxidation of ENR 50 that caused a reduction in the free volume of the chain phases, hence stiffening the molecular chain structure, as noted by Yusoff *et al.* [11]. Thus, the ENR 50 film was not further characterized by OM and EIS. The PMMA/ENR 50 and $PMMAF_0$ films (Figure 1(c) & (d)) showed improved flexibility, due to the elastomeric properties of ENR 50. Flexible and free-standing films were successfully obtained after 1 and 3 wt. % Al_2O_3

($PMMAF_1$ and $PMMAF_3$) were added to the PE systems, as shown in Figure 1(e) and (f), respectively. This might be due to the greater amorphicity of the polymer matrix due to polymer-filler interactions. However, the films obtained with the addition of ≥ 5 wt. % Al_2O_3 ($PMMAF_5$, $PMMAF_7$ and $PMMAF_{10}$) were brittle, as shown in Figure 1(g) - (i). This may be due to the agglomeration that occurred as more filler was added. Due to the brittleness of these films, EIS analysis could not be carried out.

Characterization

FTIR Studies

The FTIR spectra for pure PMMA, pure ENR 50, PMMA/ ENR 50 and $PMMAF_{0-10}$ are displayed in Figure 2.

As shown in Figure 2, the spectral peaks for pure PMMA were observed at 1724 cm^{-1}, 2952 cm^{-1} and 1438 cm^{-1} denoting C=O, C-H and -OCH_3 stretching,

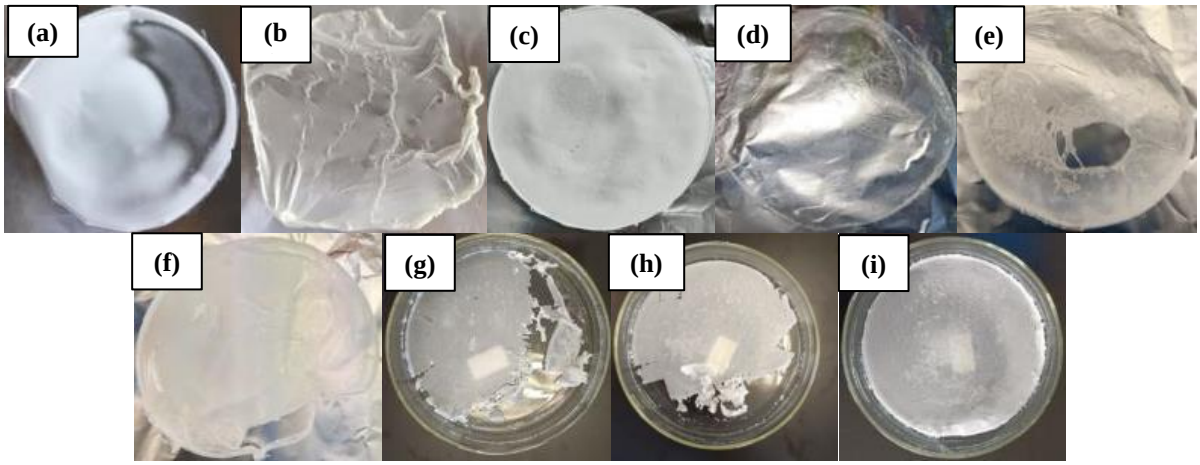

Figure 1. The films for (a) PMMA, (b) ENR 50, (c) PMMA/ ENR 50, (d) $PMMAF_0$, (e) $PMMAF_1$, (f) $PMMAF_3$, (g) $PMMAF_5$, (h) $PMMAF_7$, and (i) $PMMAF_{10}$.

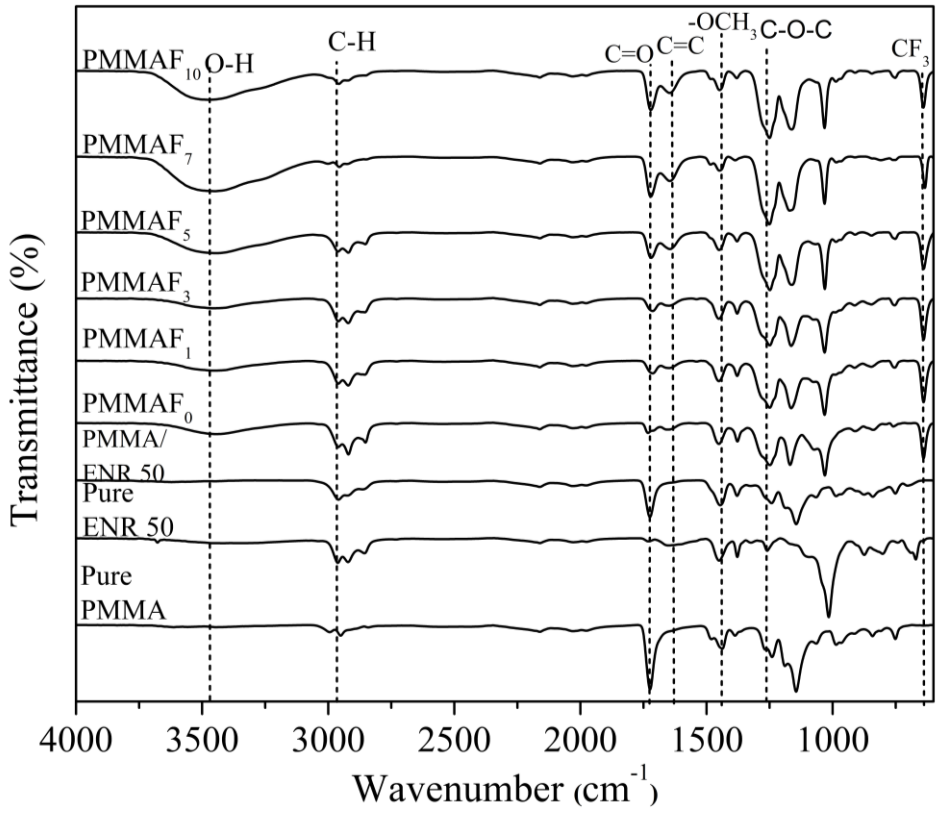

Figure 2. FTIR spectra of pure PMMA, pure ENR 50, PMMA/ENR 50 and $PMMAF_{0-10}$

respectively, which agreed with a previous study by Kushwaha *et al.* [12]. The peaks for pure ENR 50 were observed at 1249 cm^{-1} and 1650 cm^{-1} representing C-O-C and C=C stretching, respectively, which concurred with a study by Latiff *et al.* [5]. The peaks representing the coordinating sites of the polymer hosts such as the C=O and OCH_3 stretching of PMMA as well as the C-O-C stretching (epoxide group) of ENR 50 were examined in more detail. After blending ENR 50 with PMMA, a new OH stretching peak was observed at 3465 cm^{-1}, indicating a hydrogen bonding interaction between these polymers. The same observation has also been reported by Zamri *et al.* [8]. The C=O stretch of PMMA at 1724 cm^{-1} shifted to a slightly lower frequency of 1720 cm^{-1}, with a lower peak intensity. The -OCH_3 stretch at 1438 cm^{-1} and CH_3 stretch at 2952 cm^{-1} in the PMMA spectrum were found to have shifted higher to 1445 cm^{-1} and 2957 cm^{-1}, respectively. In addition, the C-O-C stretch at 1249 cm^{-1} for ENR 50 had shifted down to 1241 cm^{-1} in the PMMA/ENR 50 blend system. The changes in the wavenumbers of these peaks further confirmed the interactions between PMMA and ENR 50.

On doping the PMMA/ENR 50 blend system with LiTf salt ($PMMAF_0$), a new peak at 630 cm^{-1} representing the CF_3 stretch of the salt's triflate ion (CF_3^-) was observed. This was also reported by Azli *et al.* [13]. The C=O and -OCH_3 stretching peaks at 1720 and 1445 cm^{-1} shifted to 1732 cm^{-1} and 1451 cm^{-1} respectively, along with a reduction in peak intensities. A downshift of the C-O-C stretching peak at 1241 cm^{-1} to 1249 cm^{-1} was also detected. These observations confirmed that interactions had occurred between the oxygen atoms of PMMA and ENR 50 and the lithium cations of the salt. The OH stretching peak broadened after addition of LiTf; this represents moisture due to the hygroscopic nature of LiTf. This was further confirmed by the appearance of an OH bending peak of water at 1640 cm^{-1}. A similar observation was also reported by Tan *et al.* [14] when Li-X salts of LiTf, $LiBF_4$, $LiCOOCF_3$, LiI, and $LiClO_4$ were used in polymer systems.

Upon addition of the Al_2O_3 nanofiller, it was observed that the C=O peak shifted down from 1732 cm^{-1} in $PMMAF_0$ to 1714 cm^{-1} in $PMMAF_3$ and up to 1721 cm^{-1} in $PMMA_{10}$. The peak intensity was also observed to decrease when 1 and 3 wt. % of Al_2O_3 was added, indicating interactions between the filler and the C=O group of PMMA. According to Sownthari *et al.* [15], interactions between the filler, salt and polymer increased the amorphicity of the system. Also, Yang *et al.* [16] reported that these interactions could reduce the intermolecular forces and enhance the motion of polymer chains. This can be confirmed by the flexible films we obtained (Figure 1(e) and (f)). However, the C=O peak intensity was observed to increase with the addition of larger amounts of Al_2O_3 (5,7 and 10 wt. %); this was probably due to reduced interactions resulting from the agglomeration produced by higher filler concentrations. This theory explains the brittle and rough surfaces of the films with ≥ 5 wt. % of Al_2O_3 (Figure 1 (g)-(i)). There were no shifts in the wave-numbers observed for the -OCH_3 and C-O-C stretching peaks. The intensity of the CF_3 peak representing the salt's triflate ion increased upon addition of 1-7 wt.% of the Al_2O_3 nanofiller, indicating the presence of filler-salt interactions. Based on the FTIR analysis, the proposed interactions between the constituents of this Al_2O_3-doped PMMA/ ENR 50-based electrolyte are shown in Figure 3.

EIS Studies

Figure 4 shows the Cole-Cole plots for the PMMA/ ENR 50-based electrolyte system. The plot for PMMA/ ENR 50 (Figure 4(a)) forms a semicircle. For $PMMAF_0$ and $PMMAF_1$ (Figure 4(b) and (c)), both semicircles and spikes were observed. However, the Cole-Cole plot for $PMMAF_3$ (Figure 4 (d)) only displays a spike. The formation of a semicircle reveals the polymer electrolyte's bulk conductance, which is equivalent to the parallel combination of its bulk resistance (R_b) and bulk capacitance. The immobility of the polymer chains causes the bulk capacitance, while the presence of mobile ions in the polymer matrix causes the bulk resistance [17]. The formation of spikes for $PMMAF_0$, $PMMAF_1$ and $PMMAF_3$ is due to the charge transfer at the interface that creates a double layer capacitance. In addition, a spike also indicates the presence of ion diffusion in the samples [18].

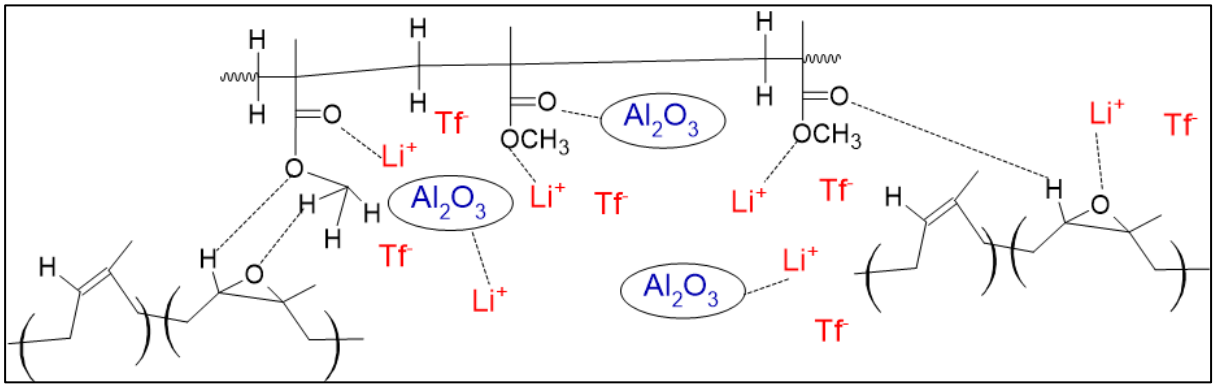

Figure 3. Proposed interactions between constituents of the Al_2O_3-doped PMMA/ENR 50-based electrolyte.

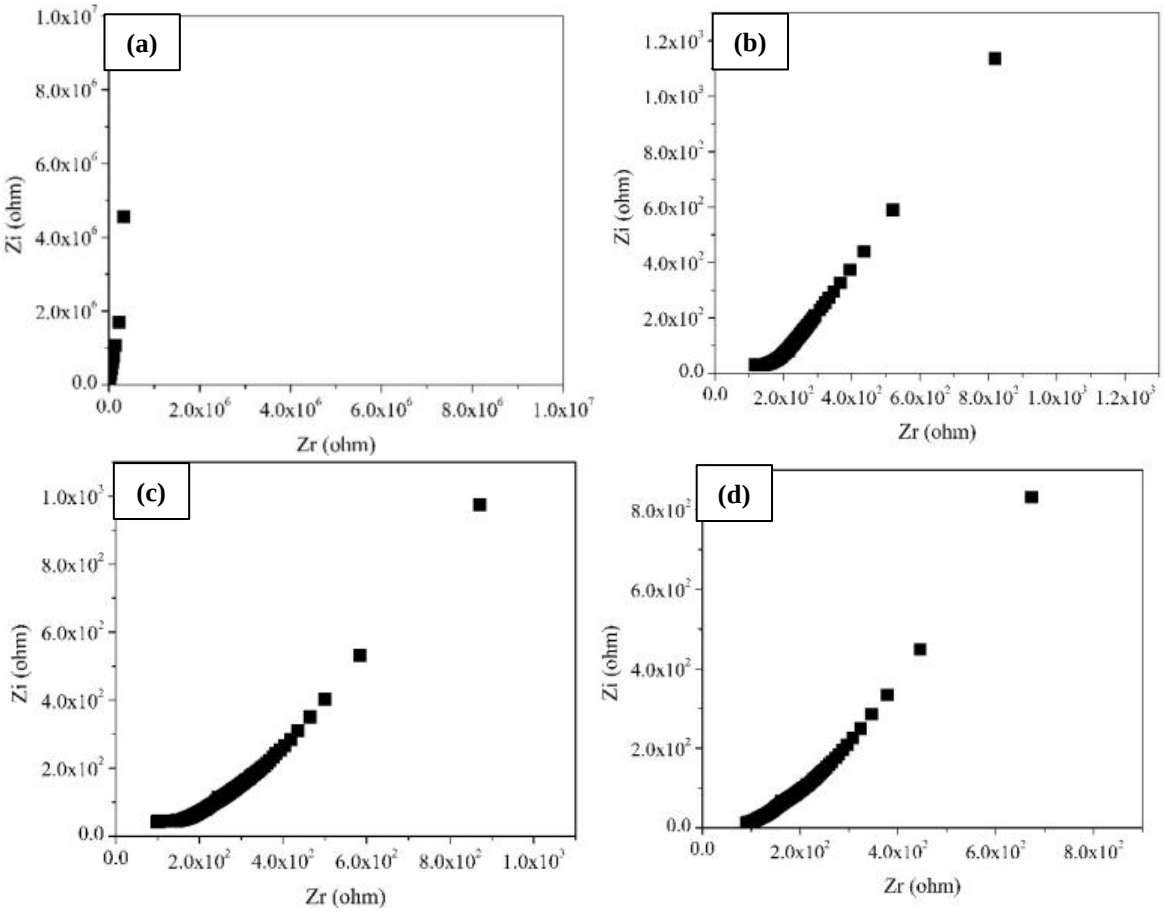

Figure 4. Cole-Cole plots for (a) PMMA/ ENR 50, (b) $PMMAF_0$, (c) $PMMAF_1$ and (d) $PMMAF_3$

Table 1 lists the ionic conductivity obtained for all the samples. The PMMA/ENR 50 film had an ionic conductivity of 5.10 x 10^{-9} S/cm. With the incorporation of LiTf, the ionic conductivity of the system increased to 2.21×10^{-4} S/cm. This was due to the mobility of the charge carrier (Li^+ ions) in the system. After adding 1 and 3 wt. % of Al_2O_3 ($PMMAF_1$ and $PMMAF_3$), the ionic conductivity of the films increased to 2.46×10^{-4} S/cm and 4.36×10^{-4} S/cm respectively. The increase in ionic conductivity may be caused by two factors:

(i) The increase in the amorphicity of the system due to polymer-filler interactions, as confirmed by FTIR analysis. The amorphous phase eases the mobility of Li^+ ions, which explains the improved ionic conductivity with filler incorporation.

(ii) The creation of new conducting pathways for Li^+ ions due to filler-salt interactions, as confirmed by FTIR. This in turn improves ionic transportation in the polymer electrolyte [19].

Table 1. The ionic conductivity of PMMA/ENR 50-based electrolyte films.

Samples	Average Ionic Conductivity (S/cm)	Standard Deviation
PMMA/ ENR 50	5.10×10^{-9}	$\pm 3.21\times 10^{-9}$
$PMMAF_0$	2.21×10^{-4}	$\pm 0.10\times10^{-4}$
$PMMAF_1$	2.46×10^{-4}	$\pm 0.20\times10^{-4}$
$PMMAF_3$	4.36×10^{-4}	$\pm 0.21\times10^{-4}$

Table 2. Ionic conductivities of other PMMA-based filler incorporated polymer electrolytes.

Polymer system	Weight Percentage of Filler (%)	Conductivity (S/cm)	References
PMMA/ ENR 50/LiTf	3 wt. % Al_2O_3 (<50 nm)	4.36×10^{-4}	This study
PMMA/ ENR 50/$LiBF_4$	5 wt. % SiO_2 (15 nm)	5.30×10^{-6}	[20]
PEO/PMMA/LiTFSI	Al_2O_3 (10 nm) (Unreported wt. %)	9.37×10^{-7}	[22]
PEO/PMMA/$LiClO_4$	3 wt. % Al_2O_3 (<50 nm)	4.90×10^{-6}	[23]

Table 2 shows the ionic conductivities obtained from other filler-doped PMMA blend electrolyte systems. It is clear that the system developed in this study showed a remarkably higher ionic conductivity than other filler-doped PMMA blend electrolyte systems. This system also exhibited conductivity values up to two orders of magnitude higher than the values reported by Zamri *et al.* [20], who used a smaller sized SiO_2 filler. This was due to the formation of Si-OH (silanol) groups which inhibited ion movement in the polymer electrolyte system. This proves that Al_2O_3 has less tendency to react with surrounding moisture compared to SiO_2, because aluminium (Al) is more electropositive than silicon (Si) [21].

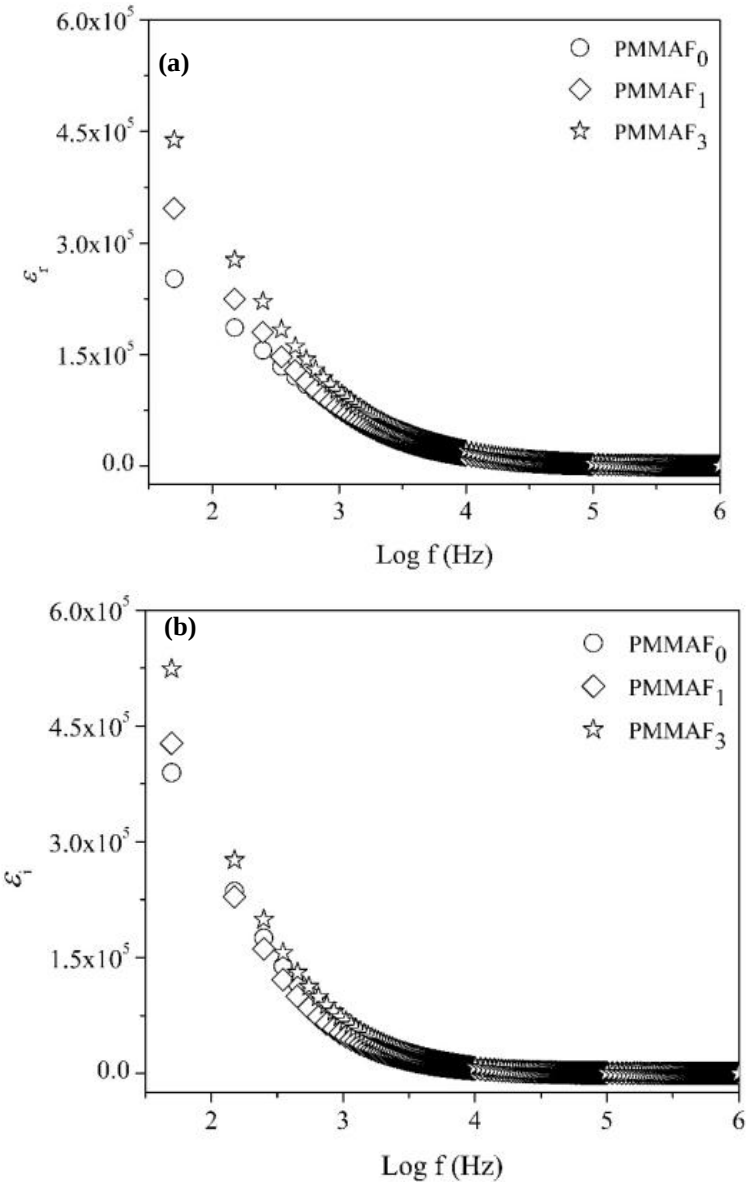

Figure 5. Dielectric studies of (a) ε_r vs log f and (b) ε_i vs log f for $PMMAF_{0\text{-}3}$.

A dielectric study for PMMA/ENR 50-based polymer electrolytes with different wt. % of Al_2O_3 was conducted to better understand the nature of ionic transport in this system. Figure 5(a) and (b) show the plots of dielectric constant (ε_r) and dielectric loss (ε_i) as a function of log f, respectively. High values of ε_r and ε_i were observed at low frequencies, which indicate the association of charge carriers or polarization effects at the electrode-electrolyte interface before the electric field changed direction [24]. The reversal rate of the electric field increases at high frequencies, and this provides no time for the charges to accumulate at the interface, resulting in low ε_r and ε_i values [25]. The highest ε_r and ε_i values were obtained at the highest ionic conductivity of $PMMAF_3$. This was because more energy had been used to align a higher number of charges in the system.

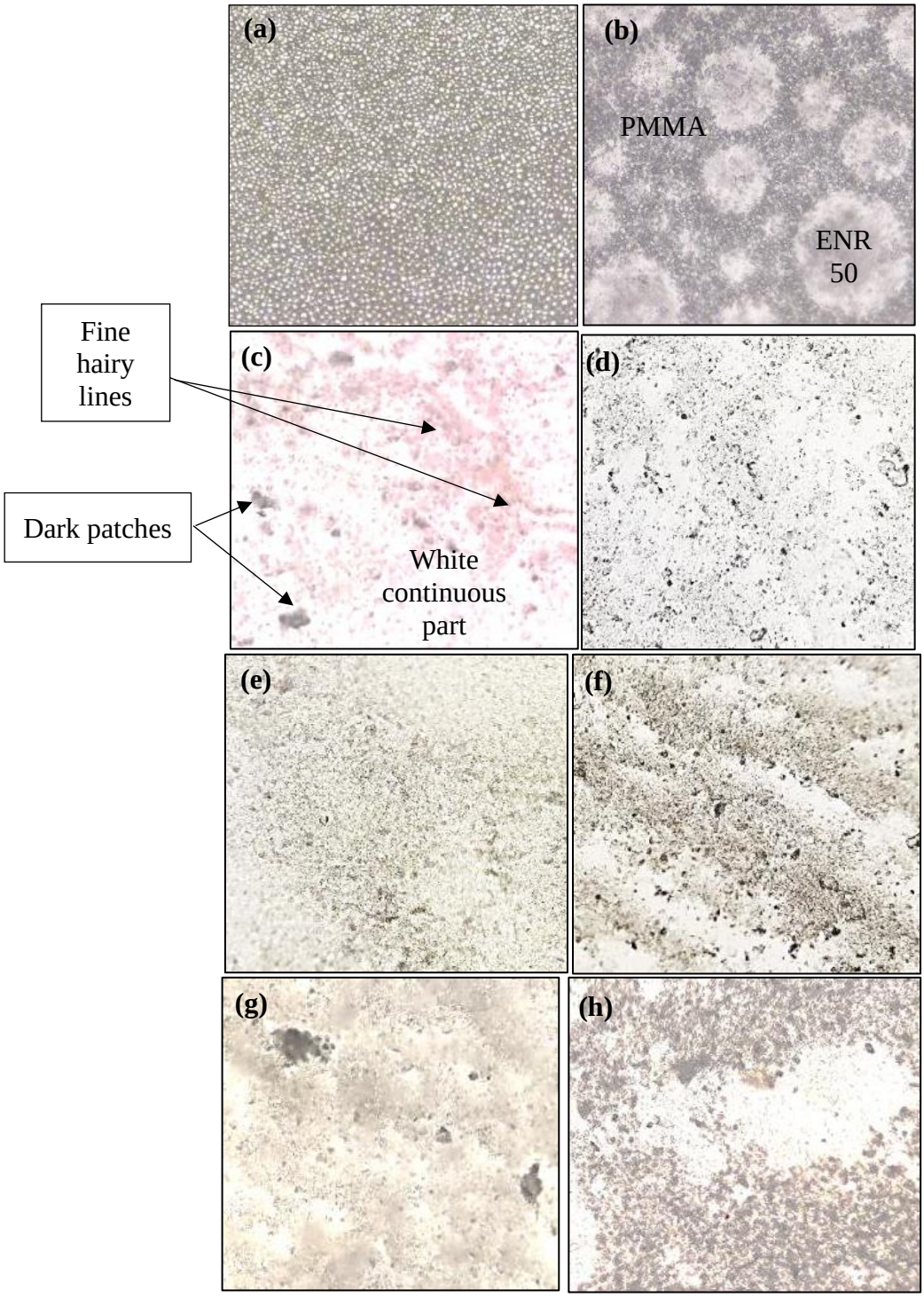

Figure 6. Optical micrographs of (a) PMMA, (b) PMMA/ENR 50, (c) $PMMAF_0$, (d) $PMMAF_1$, (e) $PMMAF_3$, (f) $PMMAF_5$, (g) $PMMAF_7$, and (h) $PMMAF_{10}$.

OM Studies

The pure PMMA film in Figure 6(a) displayed a rough surface with uniformly distributed spherical grains which explained its brittleness due to restricted chain flexibility. The morphology of the PMMA/ENR 50 film (Figure 6(b)) showed phase separation that indicated its inhomogeneity. After adding LiTf, the grains disappeared, as in Figure 6(c) ($PMMAF_0$). This is due to the interaction of the oxygen atoms of PMMA with Li^+ ions of the doping salt, as confirmed by FTIR analysis. Figure 6(c) also shows dark patches indicating a topological disorder resulting from the random distribution and dissociation of LiTf salts [26]. In addition, the two-phase separation of PMMA/ENR 50 could still be seen. The white continuous parts represent the PMMA-rich phase, while the fine hairy lines represent the ENR 50-rich phase of the film. The same observations were also reported by Zamri *et al.* [8] for a PMMA/ENR 50-based electrolyte film.

Figure 6(d) & (e) show the morphology of the films with 1 and 3 wt. % Al_2O_3 ($PMMAF_{1-3}$). It was clear that phase separation no longer occurred, suggesting that there was no blocking phase and ions could move quickly. Moreover, the smooth film surface indicated a uniform and homogenous distribution of the Al_2O_3 nanofiller in the whole polymer salt matrix. This is probably due to the ability of Al_2O_3 to occupy the spaces between PMMA and ENR 50, hence forcing ENR 50 to move into the PMMA phase. The same observation was also reported when SiO_2 filler was added to a PMMA/ENR 50-based electrolyte [8].

With the addition of ≥ 5 wt. % of Al_2O_3, the films showed agglomeration due to the high concentration of fillers (Figure 6(f) – (h)) which further confirmed the observations from FTIR analysis. In addition, the film surfaces became rougher. The agglomeration of Al_2O_3 lead to an increase in crystallinity of the polymer matrices, which was confirmed by the brittle nature of the $PMMA_{5-10}$ films (Figure 1(g) – (i)).

TGA Studies

The thermogravimetric (TG) curves of $PMMAF_0$, $PMMAF_1$ and $PMMAF_3$ are depicted in Figure 7. The TG curves for $PMMAF_{0-3}$ showed four decomposition temperatures (T_d). The first three T_d are related to the decomposition of PMMA as previously reported by Zailani *et al.* [27]. The first degradation stage was due to the decomposition of weak head-to-head linkages and impurities trapped inside PMMA. The second stage of deterioration was due to the breakdown of its side chain, while the third stage was due to the break-down of the main chain of PMMA [27]. The fourth stage may be due to the decomposition of LiTf. Interestingly, the degradation temperatures observed for $PMMAF_1$ and $PMMAF_3$ were higher than that of $PMMAF_0$ which suggested that the incorporated Al_2O_3 significantly increased the thermal stability of the PMMA/ENR 50-based electrolyte system. This is likely due to the interactions between the filler and the C=O group of PMMA, as confirmed by FTIR analysis.

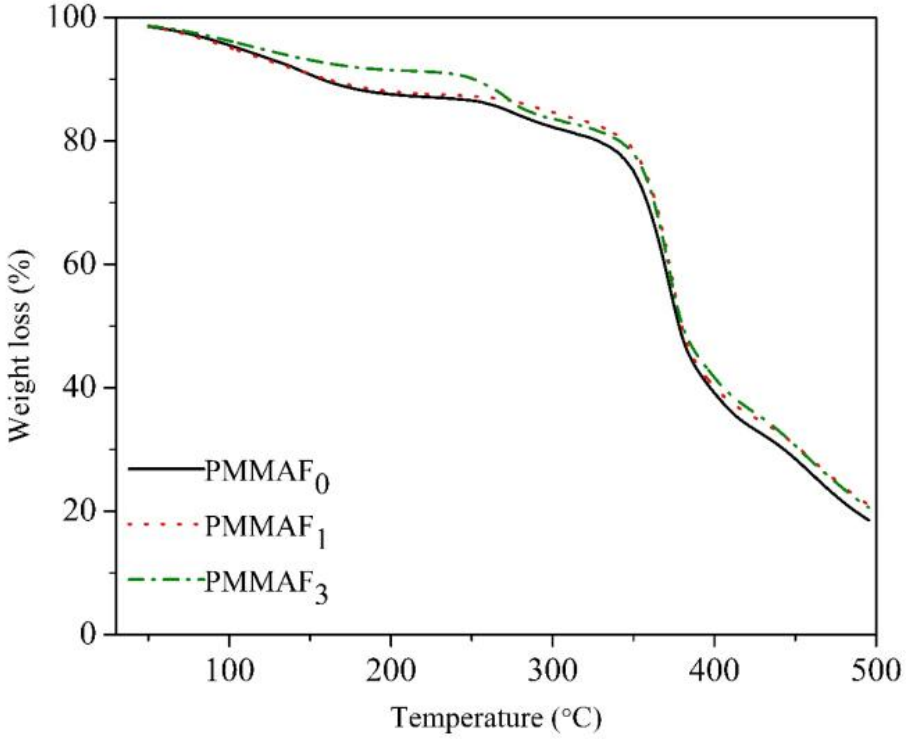

Figure 7. TG curves of $PMMAF_{0-3}$.

CONCLUSION

Flexible, free-standing PMMA/ENR 50-based electrolyte films with improved homogeneity were obtained by the addition of up to 3 wt. % of Al_2O_3. This was confirmed by the smooth and homogenous morphology of the $PMMAF_1$ and $PMMAF_3$ films observed via OM. This is probably due to the ability of Al_2O_3 to occupy the spaces between PMMA and ENR 50, which forced ENR 50 to move into the PMMA phase. FTIR analysis confirmed that there were interactions between the oxygen atoms of the PMMA-based electrolyte and the coordination sites of ENR 50, LiTf and Al_2O_3. These interactions successfully increased the amorphicity of the system, which allowed flexible films to be formed. The increased amorphicity also eased the mobility of the Li^+ ions, as proven by the highest ionic conductivity value of 4.36×10^{-4} S/cm obtained for $PMMAF_3$. The filler-salt interactions also increased conductivity by creating new Li^+ conducting pathways. Interestingly, the $PMMAF_1$ and $PMMAF_3$ also exhibited higher decomposition temperatures compared to $PMMAF_0$ which may be related to the PMMA-filler interactions, as confirmed by FTIR analysis. This system has potential to be applied in lithium-ion batteries due to its good ionic conductivity. Further studies on the temperature-dependence of conductivity should be carried out to specifically investigate the ion conduction mechanism of the system.

ACKNOWLEDGEMENTS

The authors are very grateful to the Faculty of Applied Sciences, UiTM Perlis branch for their support of this research. Thanks also goes to the MyRA Lepasan PhD grant (600-RMC/GPM LPHD 5/3 (084/2022) and 600-RMC/GPM LPHD 5/3 (121/2021)) for the financial assistance.

REFERENCES

1. Droguet, L., Grimaud, A., Fontaine, O. & Tarascon, J. (2020) Water-in-Salt Electrolyte (WiSE) for Aqueous Batteries: A Long Way to Practicality. *Advance Energy Materials*, **10**, 2002440.

2. Zhu, M., Wu, J., Wang, Y., Song, M., Long, L., Siyal, S. H., Yang, X. & Sui, G. (2019) Recent advances in gel polymer electrolyte for high-performance lithium batteries. *Journal of Energy Chemistry*, **37**, 126–142.

3. Basri, N. D., Latif, F. A., Ibrahim, R., Ghani, F. S. A. & Zamri, S. F. M. (2021) Formation, morphological, molecular interaction and ionic conductivity of SiO_2 filled PMMA/PEG electrolytes. *Malaysian Journal of Analytical Sciences*, **25(2)**, 234–242.

4. Gohel, K. & Kanchan, D. K. (2019) Effect of PC: DEC plasticizers on structural and electrical properties of PVDF–HFP: PMMA based gel polymer electrolyte system. *Journal of Materials Science: Materials in Electronics*, **30(13)**, 12260–12268.

5. Latif, F., Zamri, S. F. M. & Aziz, M. (2015) Anions effect on the electrical properties of PMMA/ ENR 50 blend electrolytes. *Advanced Materials Research*, **1107**, 145–150.

6. Brydson, J. A. & Gilbert, M. (2016) *Brydson's Plastics Materials*. Butterworth-Heinemann.

7. Zamri, S. F. M. & Latif, F. A. (2013) SiO_2 filler as interface modifier in PMMA/ENR 50 electrolytes. *Advanced Materials Research*, **812**, 120–124.

8. Zamri, S. F. M., Latif, F. A., Ali, A. M. M., Ibrahim, R., Azuan, S. I. H. M., Kamaluddin, N. & Hadip, F. (2018) Filler and polymer interactions in polymethyl methacrylate/50% epoxidized natural rubber/silicon dioxide nanocomposites. *Malaysian Journal of Analytical Sciences*, **22(4)**, 586–593.

9. Tang, C., Hackenberg, K., Fu, Q., Ajayan, P. M. & Ardebili, H. (2012) High ion conducting polymer nanocomposite electrolytes using hybrid nanofillers. *Nano letters*, **12(3)**, 1152–1156.

10. Latif, F., Aziz, M., Katun, N. & Yahya, M. Z. (2006) The role and impact of rubber in poly (methyl methacrylate)/lithi triflate electrolyte. *Journal of Power Sources*, **159(2)**, 1401–1404.

11. Yusoff, S. N. H. M., Har, S. L., Han, C. C., Hashifudin, A. & Kammer, H. W. (2013) Solid solution of polymer electrolytes based on modified natural rubber. *Polymers Research Journal*, **7(2)**, 159.

12. Kushwaha, A. K., Gupta, N. & Chattopadhyaya, M. C. (2017) Dynamics of adsorption of Ni (II), Co (II) and Cu (II) from aqueous solution onto newly synthesized poly [N-(4-[4-(aminophenyl) methylphenylmethacrylamide])]. *Arabian Journal of Chemistry*, **10(2)**, S1645–S1653.

13. Azli, A. A., Manan, N. S. A. & Kadir, M. F. Z. (2015) Conductivity and dielectric studies of lithium trifluoromethanesulfonate doped polyethylene oxide-graphene oxide blend based electrolytes. Advances in Materials Science and Engineering.

14. Tan, W. L., Abu Bakar, M. & Abu Bakar, N. H. H. (2013) Effect of anion of lithium salt on the property of lithium salt-epoxidized natural rubber polymer electrolytes. *Ionics*, **19(4)**, 601–613.

15. Sownthari, K. & Austin Suthanthiraraj, S. (2015) Influence of Al_2O_3 nanofiller on the properties of polymer electrolyte based on poly-ε-caprolactone. *Polymer Bulletin*, **72(1)**, 61–73.

16. Yang, X., Liu, J., Pei, N., Chen, Z., Li, R., Fu, L. & Zhao, J. (2023) The critical role of fillers in composite polymer electrolytes for lithium battery. *Nano-Micro Letters*, **15(1)**, 74.

17. Naik, J., & Bhajantri, R. F. (2018) Impact of ceria nanofillers on temperature dependent electrical and transport properties of PVA solid polymer electrolyte films. *Materials Research Express*, **5(6)**, 065310.

18. Tang, W., Tang, S., Zhang, C., Ma, Q., Xiang, Q., Yang, Y. W. & Luo, J. (2018) Simultaneously enhancing the thermal stability, mechanical modulus, and electrochemical performance of solid polymer electrolytes by incorporating 2D sheets. *Advanced Energy Materials*, **8(24)**, 1–3.

19. Sun, C. C., You, A. H., Teo, L. L. & Thong, L. W. (2018) Effect of Al_2O_3 in poly (methyl methacrylate) composite polymer electrolytes. *AIP Conference Proceedings*, **1958(1)**, 020028.

20. Zamri, S. F. M., Latif, F. A., Ali, A. M. M., Ibrahim, R., Azuan, S. I. H. M., Kamaluddin, N. & Hadip, F. (2017) Exploration on effects of 15 nm SiO_2 filler on miscibility, thermal stability and ionic conductivity of PMMA/ENR 50 electrolytes. *AIP Conference Proceedings*, **1809(1)**, 020049.

21. Sengwa, R. J., Choudhary, S. & Dhatarwal, P. (2019) Investigation of alumina nanofiller impact on the structural and dielectric properties of PEO/PMMA blend matrix-based polymer nano-composites. *Advanced Composites and Hybrid Materials*, **2(1)**, 162–175.

22. Liang, B., Tang, S., Jiang, Q., Chen, C., Chen, X., Li, S. & Yan, X. (2015) Preparation and characterization of PEO-PMMA polymer composite electrolytes doped with nano-Al_2O_3. *Electrochimica Acta*, **169**, 334–341.

23. Choudhary, S. & Sengwa, R. J. (2017) Effects of different inorganic nanoparticles on the structural, dielectric and ion transportation properties of polymers blend based nanocomposite solid polymer electrolytes. *Electrochimica Acta*, **247**, 924–941.

24. Aziz, S. B., Abdullah, O. G. & Al-Zangana, S. (2019) Solid polymer electrolytes based on chitosan: NH_4Tf modified by various amounts of TiO_2 filler and its electrical and dielectric characteristics. *Int. J. Electrochem. Sci*.,**14**, 1909–1925.

25. Ganta, K. K., Jeedi, V. R., Katrapally, V. K., Yalla, M. & Emmadi, L. N. (2021) Effect of TiO 2 Nano-Filler on Electrical Properties of Na+ Ion Conducting PEO/PVDF Based Blended Polymer Electrolyte. *Journal of Inorganic and Organo-metallic Polymers and Materials*, **31**, 3430–3440.

26. Noor, S. A. M., Ahmad, A., Talib, I. A. & Rahman, M. Y. A. (2009) Characterization of PEO-ENR 50 based solid polymer electrolyte. *In Prosiding Seminar Kimia Bersama UKM-ITB VIII*, **9(11)**.

27. Zailani, N. A. M., Latif, F. A., Ali, A. M. M., Rani, M. A. A. & Yahya, M. Z. A. (2018) Synthesis of flexible acrylates films. In *AIP Conference Proceedings*, **2030(1)**, 020119.